Resonances in low-energy electron scattering from *para*-benzoquinone

Journal Name

ARTICLE TYPE

Cite this: DOI: 10.1039/xxxxxxxxxx

Resonances in low-energy electron scattering from *para*-Benzoquinone

Alexandra Loupas,[a,b] and Jimena D. Gorfinkiel[a]

Received Date
Accepted Date

DOI: 10.1039/xxxxxxxxxx

www.rsc.org/journalname

We present detailed *ab initio* scattering calculations for electron collisions with *para*-benzoquinone. The *R*-Matrix method has been used to study elastic and electronically inelastic scattering. We have identified 26 resonances of Feshbach, core-excited shape and mixed character between 0 and 8 eV. Agreement of our resonance spectrum with existing literature is discussed, in particular that of the low-lying resonances that participate in the photodetachment process. Integral elastic and total inelastic cross sections are also presented.

1 Introduction

Over the last two decades, computational and experimental studies of low energy electron interactions with biological molecules have been carried out by a number of groups [1]. DNA constituents and their derivates have been the main focus of these studies. Experimental work confirmed that, below the ionization threshold, single and double DNA strand breaks occur via dissociative electron attachment (DEA) [2]. The first step in DEA is the formation of a temporary negative ion or resonances. Therefore, the identification and characterisation of these resonances constitutes an essential step to understand the DEA process. Much theoretical work has therefore been carried out in this area. Other constituents of biological micromolecules (e.g. amino acids) as well as targets of interest because of their radiosensizing properties (e.g. cisplatin) have also been studied. [3] However, the scattering community has paid significantly less attention to other types of biomolecules.

In this paper, we report the study of electron collisions from *para*-benzoquinone ($C_6H_4O_2$, 1,4-benzoquinone or *p*-BQ), the prototypical member of the quinone family; the emphasis of the work is on the identification and characterization of shape and core-excited resonances. Quinones are commonly found in nature and play a crucial role in electron transfer reactions in chemistry and biology [4,5], for example in photosynthesis. [6] From the biochemical point of view, there are several natural and synthetic quinones known by their antitumoral activity [7,8], whilst others are involved as redox cofactors in quinoenzymes [9,10]. Fundamental insights into the mechanism of electron capture by quinones were obtained from the experimental studies of *p*-BQ, for example those performed by Cook *et al.*, who studied for the first time the fluorescence from an excited state of the radical anion of *p*-BQ and showed the important implications of the possibility of using these states for driving chemical reactions (electron transfer) [11]. Zamadar *et al.* measured the electron transfer rates in excited benzoquinone anions in tetrahydrofuran [12] and Holroyd studied the attachment and photodetachment of *p*-BQ in different non-polar solvents. [13]

A number of photodetachment experiments are available for *p*-BQ [13–16]. Detailed studies of the ultrafast dynamics of *p*-BQ^- have been performed using time-resolved photoelectron spectroscopy [17] and frequency-resolved photoelectron spectra (and asymmetry parameters) have been published. [18] These experiments prove a range of molecular geometries (five low lying resonances are understood to play an important role in the photodetachment process [18]): the energy provided by the photon can take the system into one of the temporary anionic states of *p*-BQ which will decay, through conical intersections, to the ground anionic state [17]; the dependence of the anionic states on the molecular geometry is therefore of great interest. In contrast, electron scattering at the energies studied in this work can be described reasonably well as a collision of the electron with the molecule in its (fixed) ground state equilibrium geometry (vibrational excitation is ignored; DEA requires the investigation of a large number

[a] *School of Physical Sciences, The Open University, Walton Hall, Milton Keynes, MK7 6AA, United Kingdom.*
[b] *Departamento de Física, Faculdade de Ciências e Tecnologia, Universidade Nova de Lisboa, Campus de Caparica, 2829-516, Portugal*

of geometries). Electron scattering experiments (excluding DEA), therefore, tend to probe mainly the resonances at the ground state equilibrium geometry only.

Several theoretical calculations have been performed to identify the temporary anions of *p*-BQ. These are based either on conventional (bound-state) quantum chemistry techniques or they make use of approaches specifically developed to treat transient anions (i.e. stabilization techniques or use of a complex absorbing potential). The latter can be expected to produce reasonable results for the position and width of the resonances. Standard bound variational techniques, however, are always at risk of collapse to the continuum and should therefore be interpreted in this light.

All theoretical works resonance information for the equilibrium geometry of neutral *p*-BQ (many also provide the energies of the resonant states for other geometries of interest, in particular the (bound) ground state anion equilibrium geometry). Pou-Amérigo *et al.*[19] used standard quantum chemistry approaches (CASSCF/CASPT2) to investigate resonances found in previous experiments. Honda *et al.*[20] used the SAC-CI method to identify six experimentally observed resonances of shape and Feshbach character below 5 eV. Cheng *et al.*[21] studied shape and core-excited resonances using a stabilization method. They report the energies and widths of ∼20 resonances - shape and core-excited - in the range of 0 to 6 eV. West *et al.* present results from anion frequency-resolved photoelectron imaging as well as some standard (bound state) quantum chemical calculations for the energy of six resonances in the range 0-2.4 eV[18]. Finally, Kunitsa and Bravaya[22,23] performed CAP-EOM-ES-CCSD calculations for the ^2A_u resonance[22] and used the multi-state multi-reference second order perturbation approach XMCQDPT2 approach, to investigate the bound and seven resonant states of the anion[23]. The energy order of the low-lying resonances at the equilibrium geometry of the neutral molecule varies between publications, as does the character (shape, Feshbach, mixed) of some of the resonances.[17]

To the best of our knowledge, no scattering calculations have been performed so far for *p*-BQ. However, several experiments have been carried out on electron scattering from *p*-BQ.[24–28]. Allan[25] measured time-resolved electron energy loss spectra below 5 eV and extended the energy range to investigate both vibrational and electronic excitation.[28] Cooper *et al.*[24] performed electron and Cs scattering measurements (the latter to determine the electron affinity of *p*-BQ). Interestingly, electron scattering from the *p*-BQ anion has also been studied[29].

In this work, we have used the well established *R*-matrix method[30] to study of elastic and inelastic low energy collisions between an electron and *p*-BQ. We have performed detailed calculations for the equilibrium geometry of the neutral and identified a large number of resonances. Positions, widths and the parent states of the resonances (when possible) are provided. The integral elastic and total inelastic (summed over all electronic excited states included in the calculation) are also presented.

2 Theory

2.1 The *R*-Matrix method

The *R*-matrix method is a well established scattering approach; its application to molecules has been described in detail elsewhere[31]. Here, we present a summarised description of it. All our calculations have been performed within the fixed-nuclei approximation, that is, keeping the atomic nuclei fixed. We chose the ground state equilibrium geometry of the *neutral* molecule as our geometry. We have used the UKRmol suite[32], a computational implementation of the *R*-matrix method.

The method is based on the division of configuration space into two regions, delimited by a sphere of radius α: the inner region, where correlation and exchange effects between all electrons play an important role and have to be considered; and the outer region, where exchange between the scattered electron and electrons of the target molecule can be neglected. Choosing the radius α of the *R*-matrix sphere is critical since the charge densities of the relevant *N*-electron target states and the $(N+1)$-electron configurations χ_i (see below) must be contained inside the inner region for the method to be valid.

In the inner region, we use a set of basis functions Ψ_k to describe the system of $(N+1)$-electrons:

$$\Psi_k^{N+1} = \mathscr{A} \sum_{i=1}^{n} \sum_{j=1}^{n_c} \Phi_i(\mathbf{x}_N; \hat{r}_{N+1}; \sigma_{N+1}) \frac{u_{ij}(r_{N+1})}{r_{N+1}} a_{ijk} + \sum_{i=1}^{m} \chi_i(\mathbf{x}_{N+1}) b_{ik} \quad (1)$$

where $\mathbf{x}_N$ and $\mathbf{x}_{N+1}$ stand for the spin *and* space coordinates of all $N/N+1$ electrons, respectively. σ_{N+1} stands for the spin of the scattering electron, and r_{N+1} and $\hat{r}_{N+1}$ correspond to its radial and angular coordinates respectively. The wave function Φ_i describes the ith electronic state of the *N*-electron target, as well as the angular and spin behaviour of the scattering electron. The functions $\frac{u_{ij}(r_{N+1})}{r_{N+1}}$ describe the radial part of the wave function of the scattering electron while the L^2-integrable functions χ_i are crucial for a good description of the short-range polarisation-correlation effects. $\mathscr{A}$ is the antisymmetrization operator, and the coefficients a_{ijk} and b_{ik} are determined by the requirement that the functions Ψ_k diagonalise the non-relativistic Hermitian Hamiltonian of the $(N+1)$-electron system, in the inner region.[31]

In the outer region, the interaction between the scattering electron and the target molecule is approximated by a single-centre multiple potential expansion. The basis functions Ψ_k^{N+1} are used to construct the *R*-matrix at the boundary between the regions. This R-matrix is propagated to the asymptotic region, where by matching with known asymptotic expressions, the *K*- matrix is determined. From the *K*- matrix one can extract resonance pa-

rameters (energy and width) as well as determine cross sections via the T-matrices.

The choice of target electronic states and the type of the L^2 functions included in the expansion (1) defines what we call the scattering model. We use the Static-Exchange plus Polarization (SEP) and close-coupling (CC) models. At the SEP level, only the target ground state wavefunction is included in expansion (1). The molecule is allowed to be polarized by the incoming electron; this effect is described by inclusion of the appropriate L^2 configurations. We include:

$$\begin{aligned} \chi_i &: (core)^{N_c}(valence)^{N-N_c}(virtual)^1 \\ \chi_i &: (core)^{N_c}(valence)^{N-N_c-1}(virtual)^{1+1} \end{aligned} \quad (2)$$

In these configurations, the core orbitals of the molecule are always doubly occupied by N_c electrons. Single excitations from the valence space (defined here as those orbitals of the ground state configuration that are not core orbitals) to a selected number of virtual orbitals, which are also available for the incoming electron, are allowed. SEP models describe shape resonances, in which the electron attaches to the molecule in the ground state, very well. The method can also describe, poorly, core-excited resonances associated with single excitations of the target molecule (some of the configurations required for the description of core-excited resonances are included in the secon set of functions described by equation (2)). When using this method, the target molecule is described at HF level.

In the more sophisticated CC approximation, a number of target electronic excited states are included in expansion (1). These are normally described at the complete active space (CAS) level. In this case, the L^2 configurations take the following form:

$$\begin{aligned} \chi_i &: (core)^{N_d}(CAS)^{N-N_d+1}, \\ \chi_i &: (core)^{N_d}(CAS)^{N-N_d}(virtual)^1. \end{aligned} \quad (3)$$

Here, the active space includes both occupied and unoccupied orbitals of the ground state configuration (therefore, the virtual space is different to that of the SEP L^2 configurations).

In these calculations, one should always be careful with balance - the description of the N electron target electronic states $\Phi_i(x_N)$ and the $N+1$ electron basis functions Ψ_k^{N+1} of the scattering system should be of the same quality. This requirement must be reflected in the choice of the target configuration interaction (CI) model and the L^2 functions to be included in equation (1). In particular, the number of virtual orbitals used for the χ_i should be such that the Ψ_k^{N+1} are not overcorrelated.[33]

2.2 Resonance identification and characterization

An isolated resonance in an electron-molecule collision manifests itself in the eigenphase sum, $\delta_{sum}(E)$, as a characteristic jump by approximately π radians[34]. This behaviour can be approximated by the Breit-Wigner formula:

$$\delta_{sum}(E) = \delta_r + \delta_{bg} = -\arctan\frac{\Gamma/2}{E-E_r} + \delta_{bg} \quad (4)$$

where E_r and Γ are, respectively, the position and width of the resonance and δ_{bg} is the background non-resonant contribution to the eigenphase sum, weekly dependent on energy. We note that a resonance is not always clearly visible in the cross section (for example, core-excited resonances may not be observed in the elastic cross section). When the background contribution varies significantly with energy or many (and/or overlapping) resonances are present, the Breit-Wigner formula is no longer a good approximation and characterizing the resonances using the eigenphase sum is very hard. We have therefore used the analysis of the time-delay, which proved to be extremely effective in recent work on similar target molecules[35], to identify and characterize resonances.

The time-delay analysis makes it easier to fully separate resonances from the background and also from each other. In this paper, we used the definition of time-delay as formulated by Smith[36] and calculated it directly from the S-matrix generated in the UKRmol suite using (a simple expression relates the eigenphase sum to the trace of the Q-matrix .[36]):

$$\mathbf{Q}(E) = \hbar\mathbf{S}\frac{d\mathbf{S}}{dE} \quad (5)$$

The analysis of the positive eigenvalues and the associated eigenvectors of the Q-matrix allow us to determine E_r and Γ: time-delays much larger than $\hbar/E$ are attributed to resonant processes and, when plotted as a function of the electron scattering energy, have the shape of a Lorentzian function. Excitation thresholds also appear as very narrow peaks in the time-delay that can interfere in the identification of resonances. (At threshold energies the incoming electron has just enough energy to excite a specific electronic state and therefore loses virtually all of its kinetic energy, causing a significant time-delay in the collision.)

The analysis of the time-delay also allows us to characterize the resonances in terms of their parent state(s). The square $|c_j|^2$ of the j-th coefficient of the eigenvectors of $\mathbf{Q}(E)$ corresponding to a resonance is equal to the branching ratio. This quantity gives the probability of decay of a metastable state into the j-th channel, and consequently, can be used to determine the parent states of shape and core-excited shape resonances.

3 Characteristics of the calculation

p-BQ is planar and belongs to the D_{2h} point group (see Figure 1), so it possesses no dipole moment; it contains N=56 electrons.

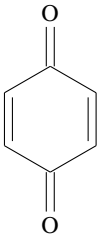

Fig. 1 Molecular structure of *p*-benzoquinone

In our calculations we have used the geometry described on the NIST website calculated at MP2 level using the cc-pVDZ basis set.[37] The main ground state configuration of *p*-BQ is $1a_g^2\ 1b_{1u}^2\ 2a_g^2\ 2b_{1u}^2\ 3a_g^2\ 1b_{2u}^2\ 3b_{1u}^2\ 1b_{3g}^2\ 4a_g^2\ 4b_{1u}^2\ 5a_g^2\ 2b_{2u}^2\ 5b_{1u}^2\ 2b_{3g}^2\ 6a_g^2\ 7a_g^2\ 6b_{1u}^2\ 3b_{2u}^2\ 4b_{2u}^2\ 7b_{1u}^2\ 8a_g^2\ 1b_{3u}^2\ 1b_{2g}^2\ 3b_{3g}^2\ 5b_{2u}^2\ 4b_{3g}^2\ 2b_{3u}^2\ 1b_{1g}^2$. The experimentally determined ionisation energy of the system is 9.9 eV[38] and its experimental polarizability is 11.23 Å^3.[39]

The description of core-excited resonances requires inclusion of electronic excited states in the scattering calculation. These excited states have been extensively studied in *p*-BQ using theoretical methods.[40–43] For the energy range we are interested in (0-8 eV), these studies report most states have valence character. The work of Pou-Amérigo *et al.*[40] provides the basis for the description of the electronic excited states in our scattering calculations.

3.1 Target model

We have performed Hartree-Fock (HF) and state-averaged CASSCF calculations (SA-CASSCF), using a compact basis set cc-pVDZ and the MOLPRO suite[44]. This basis set was selected as providing better excitation thresholds than the 6-311G** and 6-311++G** ones (the changes in these energies were relatively small). The ground state energies obtained were -379.257942164 and -379.376669703 Hartree, respectively.

In the SA-CASSCF calculations, we used the active space (12,10) (12 electrons distributed among 10 orbitals) that includes the 4 π and 4 π^* orbitals corresponding to double bonds, plus two non-bonding orbitals of the oxygen atoms. Use of a larger active space made the scattering calculations too big. We included in our state averaging 8 states - $1^1A_g\ 1^1B_{3u}\ 1^1B_{1g}\ 1-2^1B_{1u}\ 1-2^1B_{3g}\ 1^1A_u$. The vertical excitation (VE) energies of all the states included in the close-coupling expansion are listed in Table 1. Agreement is, in general, better with the results obtained by Pou-Amérigo's *et al.* at CASSCF than CASPT2 level, though our excitation energies tend to be between the two values and occasionally closer to the CASPT2 ones (Pou-Amérigo's *et al.* used a slightly different geometry; the small changes in the geometry lead to the changes in the excitation thresholds of ∼0.5 eV, even for the lowest excited states). The energies of Schreiber *et al.*[43], calculated at CASPT2 level, are lower than Pou-Amérigo's *et al.*'s. Agreement with experimental data (see Table 1) is, at best, fair.

Table 1 Vertical excitation thresholds obtained in this work from CASSCF calculations for the cc-PVDZ basis sets compared with those of Pou-Amérigo *et al.*[40] obtained from CASPT2 and CASSCF calculations and Scheiber *et al.* obtained also from CASPT2 calculations[43]. ES stands for Excited State and the energies are in eV. Also included are available experimental results[45–49].

	Pou-Amerigo		Schreiber	Exp.	This work
ES	CASPT2	CASSCF	CASPT2	-	cc-pVDZ
1^3B_{1u}	2.91	3.41	2.99	-	2.958
1^3A_u	2.27	3.55	2.68	2.32[45,47], 2.35[46]	3.158
1^3B_{1g}	2.17	3.53	2.63	2.28[45], 2.31[46]	3.163
1^1A_u	2.50	3.84	2.80	2.48[48]	3.309
1^1B_{1g}	2.50	3.88	2.78	2.48[47], 2.49[48]	3.326
1^3B_{3g}	3.19	3.82	3.31	-	3.666
2^3B_{1u}	-	-	-	-	5.135
1^1A_g	4.41	6.17	-	-	5.135
1^3A_g	-	-	-	-	5.282
3^3B_{1u}	-	-	-	-	5.502
1^1B_{3g}	4.19	6.11	4.25	4.07[49]	5.907
1^3B_{3u}	-	-	-	-	6.153
1^3B_{2g}	-	-	-	-	6.158
2^1A_g	5.90	7.04	-	-	6.178
1^1B_{3u}	5.15	6.92	5.60	-	6.211
1^1B_{2g}	4.80	6.87	-	-	6.215
1^3A_u	-	-	-	-	6.550
2^3B_{1g}	-	-	-	-	6.551
2^1A_u	5.79	7.22	-	-	6.700
2^1B_{1g}	5.76	7.22	-	-	6.702
1^3B_{2u}	-	-	-	-	6.938
1^1B_{2u}	6.89	8.30	-	-	7.462
1^1B_{1u}	5.15	7.81	5.29	5.12[49]	7.783
3^3B_{1g}	-	-	-	-	7.854
2^3A_u	-	-	-	-	7.875
2^1B_{1u}	6.86	9.11	7.91	7.1[50]	7.950
4^3B_{1u}	-	-	-	-	7.955
3^1A_g	5.90	7.04	-	-	8.229
4^3B_{1g}	-	-	-	-	8.284
3^3A_u	-	-	-	-	8.292
3^1B_{1g}	7.33	8.44	-	-	8.336
4^1A_u	7.39	8.97	-	-	8.355
2^3B_{3g}	-	-	-	-	8.380
2^1B_{3g}	6.53	8.32	-	-	8.400
5^3B_{1u}	-	-	-	-	8.448
2^3A_g	-	-	-	-	8.605
3^3A_g	-	-	-	-	8.737
4^1A_g	7.08	9.12	-	-	8.766
2^3B_{3u}	-	-	-	-	8.845
2^3B_{2g}	-	-	-	-	8.849
2^1B_{2g}	5.49	9.37	-	-	8.931
2^1B_{3u}	8.01	8.11	-	-	8.942
3^3B_{3g}	-	-	-	-	8.956
3^3B_{3u}	-	-	-	-	9.069
3^3B_{2g}	-	-	-	-	9.078
2^3B_{2u}	-	-	-	-	9.079
3^3B_{2u}	-	-	-	-	9.377

3.2 Scattering model

The R-matrix radius was set to 13 a_0 and the continuum basis set optimised for this radius was used[51], with l=4 the largest partial wave included (inclusion of l=5 in SEP calculations lead to no significantly changes in the observed resonances). In the UKRmol suite, the continuum orbitals are Schmidt orthogonalised to the orbitals of the target; the resulting continuum orbitals then undergo a symmetric orthogonalisation in which the deletion threshold was set to 1x10^{-7}.

The 48 lowest-lying electronic states shown in Table 1- all states with VE energies up to 9.4 eV in our calculations- were included in the close-coupling expansion. However, the scattering results we present here are only up to 8 eV, as the quality of the description of the excited states decreases for higher energies.

The parameters used to generate the L^2 functions, following equations (2) and (3) are N_c=16 and N_d=44 for the SEP and CC calculations, respectively. Since it is not possible to determine *a priori* the optimal number of virtual orbitals to include in the L^2 configurations, our approach is to start by performing the calculation with the M lowest energy orbitals and increase this number until we achieve good agreement with the experimental positions of the π^* resonances[52]. Using this procedure we determined that the optimal number of virtual orbitals for the SEP calculations is 35 while all 100 are needed in the CC ones.

4 Results

Table 2 lists our values for the positions and widths of the six lowest resonances of *p*-BQ together with available theoretical and experimental data. These resonances have been extensively discussed in the literature in connection to the photodetachment process[17,18,22,23].

At first sight, it is noticeable that all experimental resonance energies are in very good agreement (the range is 0.25 eV) whereas the spread of theoretical results is much broader (up to 1.26 eV). Nonetheless, it seems clear that the symmetry assignation of the first two resonances in the experiments is swapped.

Our SEP and CC results produce the same order for these resonances (the Feshbach resonances are, of course, absent from the SEP calculation). The pure shape resonances appear lower in energy for the SEP calculation (as the polarization effects are better described; prior work[52] has shown that polarization effects are not described as well at CC level for unsaturated ring molecules with high polarizabilities) whereas the mixed shape core-excited resonances are better described by the CC model where the excited parent states of the resonances are included. Our 'best results' for the resonance parameters are therefore a combination of the SEP positions and widths for the shape resonances and the CC ones for the others. The first pure shape resonances (the 1^2A_u) is significantly narrower than shape resonances tend to be, but wider than those identified as pure Feshbach by us in this target. Our calculated width corresponds to a lifetime of around 55 fs, in excellent agreement with the value calculated by Kunitsa and Bravaya.[22] The mixed character resonances (in general not identified as such by other authors) are of similar widths to the shape resonances, the 1^2B_{1g} being the significantly narrower one.

Our positions for the two pure shape resonances calculated at SEP level are in good agreement with experiment, whereas the 2^2B_{3u} resonance appears more than 0.5 eV higher (at CC level) than the highest experimental position. This is not unexpected for two reasons: (i) the potential parent states of this resonance are approximately 0.3-0.7 eV too high in our calculations, so we expect the resonance to be shifted to higher energies by a similar amount; (ii) since this resonance has partly shape character the poorer description of polarization effects in the CC calculation would also lead to a somewhat higher resonance energy.

The agreement with the theoretical results is harder to rationalize, due to the spread of values. We note that the order of our resonances is consistent with Kunitsa and Bravaya[23] but not with that of West *et al.*[18], Pou-Amérigo *et al.*[19], Honda *et al.*[20] or Cheng *et al.*[21]. For the last three cases, our order corresponds to swapping the Feshbach resonances. We note that when analyzing the results of Cheng *et al.* we have chosen, for consistency, to compare with the resonance positions obtained with the same method (those listed at the bottom of their Table 3). The positions of the A_u shape resonance is in a good agreement with Cheng *et al.* but the width is not: our calculations, both SEP and CC, produce much narrower widths for this and almost all other resonances in Table 2.

It is important to highlight that some of the resonance energies are very sensitive to small changes in the neutral equilibrium geometry: CC calculations with a geometry optimized at HF level lead to the two shape resonances being 0.21 and 0.48 eV higher whereas the Feshbach ones were 0.61 and 0.71 eV higher; this changes the order of the resonance putting the second shape and Feshbach resonances at almost the same energy and below the first Feshbach resonance in Table 2. This might also help explain the differences in the character assignation of the resonances. Kunitsa and Bravaya[23] assign a mixed shape-Feshbach character to the 1^2B_{3u} resonance in the equilibrium geometry of the neutral but Feshbach character at the anion equilibrium geometry. We find it to be a pure shape resonance, but small changes in the geometry might lead to character mixing. Similarly, those resonance we find to be of mixed character could become purely shape resonances for slightly different geometries. This sensitivity of the resonance spectrum to small changes in geometry has already been highlighted by other authors.

The two Feshbach resonances we found are below the associated peaks described in 1999 by Schiedt *et al.*. They identified six peaks between 2.213 and 2.430 eV that they postulate are likely to correspond to vibrational features of two Feshbach reso-

Table 2 Positions and widths (in brackets) in eV of the low-lying resonances of *p*-BQ calculated at SEP and CC levels. Symm: symmetry of the resonance ; C:Character. The capital letters mean: S: shape; M: mixed shape core-excited and F: Feshbach. We also list theoretical (Cheng *et al.*[21], West *et al.*[18], Kunitsa and Bravaya[23], Pou-Amérigo *et al.*[19], Honda *et al.*[20]) and experimental (Cooper *et al.*[24], Modelli and Burrow[27] and Allan[25,28]) data available. The character of the resonances in the corresponding paper is indicated in brackets.

Sym.	E_R (Width)		C	Cheng[21]	West[18]	K&B[23]	Pou[19]	Honda[20]	Experiment
	SEP	CC							
1^2A_u	0.85 (0.012)	1.10 (0.030)	S	0.910(S) (0.346)	1.01(S)	0.56 (S)	0.91 (S)	0.83[20](S)	1.35[24] 1.43[25](S) 1.60[28](S) 1.41[27]
1^2B_{2u}	-	1.70 (8E-4)	F	1.136 (F) (0.014)	1.03 (F)	0.68 (F)	0.96 (F)	1.22 (F)	
1^2B_{3g}	-	1.75 (0.001)	F	0.956 (F) (0.042)	∼0.9	0.7 (F)	0.87 (F)	1.09 (F)	
1^2B_{3u}	1.96 (0.159)	1.90 (0.071)	S	1.587 (M) (0.351)	0.68 (S)	1.43 (M)	1.31 (M)	1.79 (S)	0.70[24] 0.72[25](S) 0.77[28](S) 0.69[27]
1^2B_{1g}	3.05 (0.007)	2.35 (0.007)	M	2.099 (F) (0.058)	-	1.73 (F)	1.99 (F)	2.66 (F)	
2^2B_{3u}	3.36 (0.058)	2.67 (0.138)	M	2.332 (M) (0.139)	1.86 (F)	2.14 (F)	1.87 (M)	2.44 (F)	1.90[24] 2.15[25](S) 2.0[28](S)

nances.[16]. The parent state of the 1^2B_{2u} resonance has been easily identified as the lowest excited state, the 1^3A_u, by looking at the R-matrix poles. This is done by finding the pole closest to the resonance, and searching for the biggest coefficient of the wave function for that pole. That coefficient is associated to a configuration that allows us to identify the parent state. (One should be careful with this method as it implies two rough approximations: the closest pole might be far from resonance and not describe it particularly well and, in choosing just the main configuration, one neglects the contribution of all the other configurations for that state). In the case of the 1^2B_{3g} resonance the identification of the parent state(s) has not been possible. Both resonances are positioned more than 1 eV below the first excitation threshold, which is unusual.

This is also the case for the mixed character resonances which should have at least two parent states: the ground state and an excited one. However, the identification of potential parent states from the configurations of the closest poles was inconsistent with the behaviour of the resonances for calculations with different amount of polarization; the branching ratios do not help in this case either as resonances of Feshbach character do not decay to their parent state.

We now proceed to the discussion of the remaining resonances. The SEP calculation revealed the presence of twelve resonances of shape, mixed shape core-excited and core-excited character, identified through the cross section and time-delay analysis (Figures 2 and 3 respectively). Although, as said before, this calculation does not include the excited states of the target molecule, it does include in the $N+1$ wave functions some of the configurations required to describe them, which allow us to observe some features that might correspond to core-excited resonances. These are more accurately described when the CC method is used, and some of them are more clearly visible in the inelastic cross section (Figure 4). The CC time-delay, plotted in Figure 5, presents, in every symmetry, some structure within the energy range 3.0-4.0 eV. Although the presence of Feshbach resonances in this region cannot be excluded, it is clear that some of the structure is due to the many thresholds in this range - see Table 1.

Table 3 summarizes the resonances positions and widths for the CC calculation, as well as the respective parent state(s). The little available theoretical and experimental data for these resonances is also listed. Not included in the table are resonances detected experimentally and for which no symmetry assignation has been attempted. For example, Modelli and Burrow identify a core-excited resonance at 2.11 eV, but do not assign it a symmetry. Similarly, they also see a band at 5.8 eV that is very likely a resonance. Allan[28] sees a very broad feature around 4.2 eV that he describes as of σ^* character and another one at 5.45 eV. Cooper *et al.*[24] reports a broad energy loss peak at 4.35 eV that they state could correspond to electronic excitation of the neutral.

Looking at the panel for the A_g symmetry in Figure 2 we can observe in the SEP cross section an extremely broad peak centered slightly above 6 eV, that could correspond to a wide resonance: the corresponding feature is visible in the time-delay. However, the CC results do not show a structure that could correspond to this one. Similarly, there is some structure above 6.5 eV, again consistent with some peaks in the time-delay that might be pseudoresonances. If we look at the inelastic A_g cross section presented in Figure 4, two clear peaks are visible (and they are also present in the in the time-delay) that, since they are absent from the SEP results, we identify as core-excited resonances. These two resonances are deemed physical and therefore included in Table 3.

At the SEP level, the B_{3u} symmetry presents four resonances clearly visible in the time-delay. The lowest two are the pure shape and mixed-character resonance already reported in Table 2. The higher two appear at lower energies in the CC calculation, that in fact shows, in the inelastic cross section, the presence of

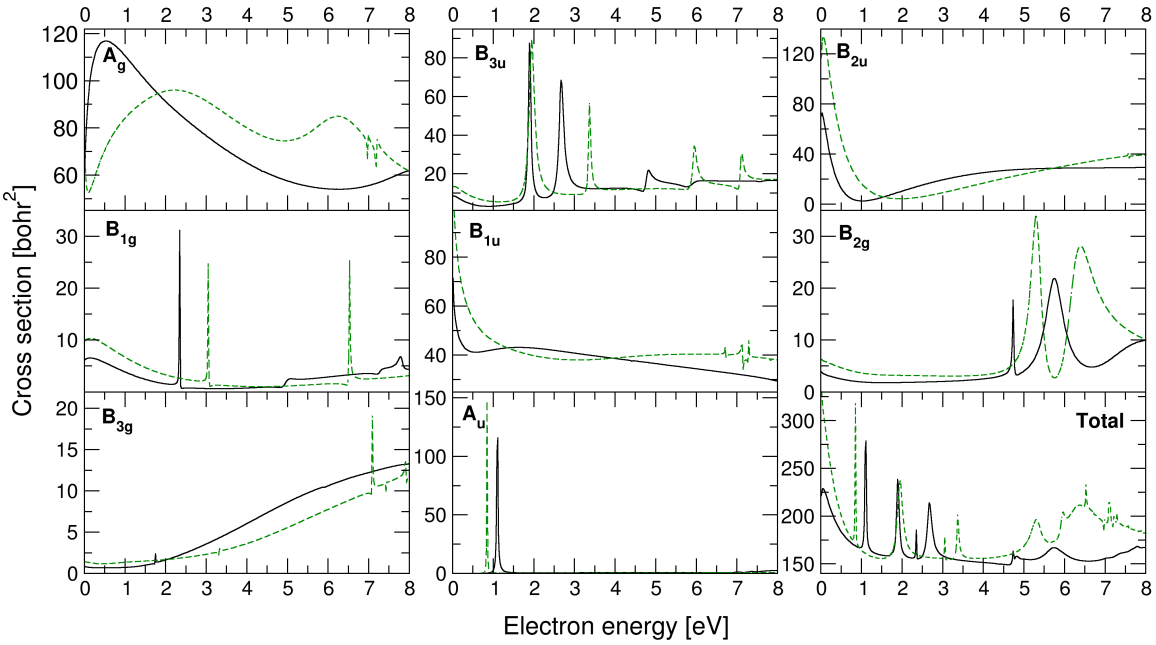

Fig. 2 Contributions to the integral elastic cross section from the scattering symmetries indicated in the panels at SEP (dashed green line) and CC level (solid black line) for the parameters described in the text. The bottom right hand panel shows the total elastic cross sections (sum of all contributions shown in the other panels) calculated at both levels.

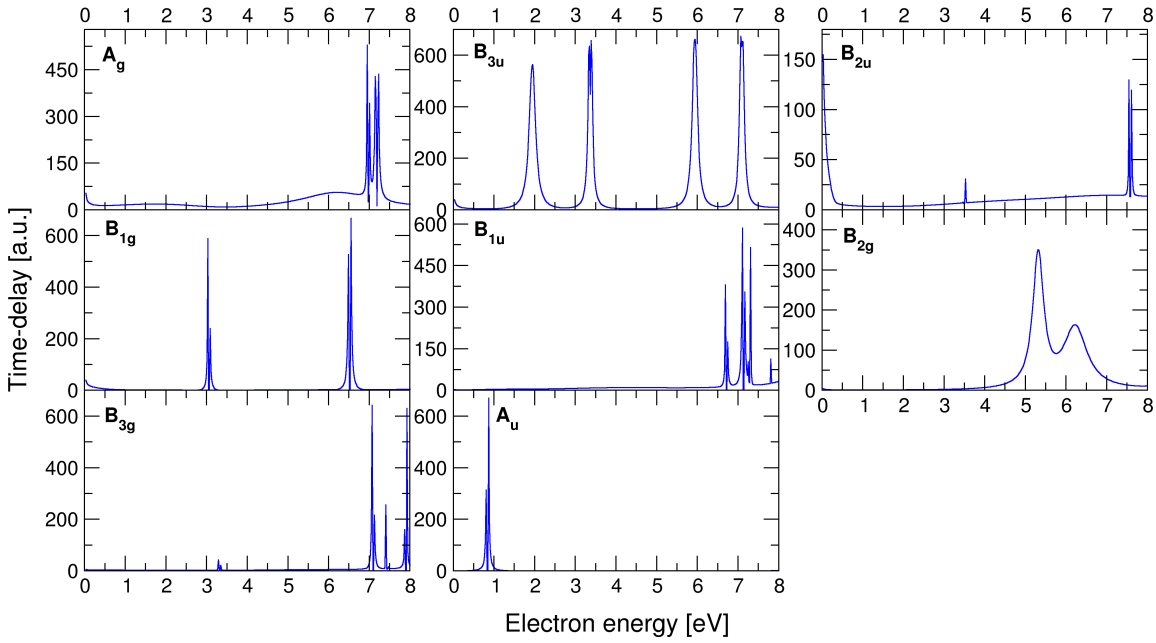

Fig. 3 Eigenvalues of the time-delay matrix for the scattering symmetries indicated in the panels at SEP level for the same parameters as in Figure 2.

a fifth resonance. This indicates these resonances have partial or whole core-excited character. The analysis of the branching ratios indicates that the resonance at 4.81 eV is of mixed shape core-excited character. Modelli and Burrow found a resonance of this symmetry at 4.37 eV that could correspond to our third resonance or to the wider one present at 5.95 eV. The calculations presented by West *et al.* [18] locate the third B_{3u} resonance at much lower energy. All these resonances are listed by Cheng *et al.* [21] as appearing at lower energies than in our calculations.

The Feshbach resonance of B_{2u} symmetry listed in Table 2 is neither visible in the CC cross section nor the time-delay with the grid we have used in Figures 4 and 5. An additional calculation with a grid four times finer was necessary to characterize it. At higher energies, the SEP calculation only shows the presence of pseudoresonances. The CC calculation shows two resonances at 5.16 eV and 6.96 eV, confirmed by time-delay. These have pure core-excited character.

The B_{1g} symmetry has one resonance reported in Table 2, visible in the elastic cross section and time-delay for both methods. As explained above, the relative positions in both methods points to a mixed shape core-excited character. The higher peak in SEP results is most likely a pseudoresonance. The elastic CC cross section shows a step at 4.97 eV, more visible as a clear peak in the inelastic cross section, and confirmed by time-delay. There are two other resonances at higher energies - 7.29 and 7.79 eV, also supported by the time-delay analysis. These 3 resonances are of pure core-excited character and the last one has not been described before.

The SEP cross sections for the B_{1u} symmetry show some structure above 6.5 eV that we identify as pseudoresonances. Even though there are no peaks in the elastic CC cross section, the inelastic one presents two peaks at 4.41 and 5.27 eV with the correspondent peaks visible in the time-delay. These resonances are assigned as pure core-excited and are also observed by Cheng *et al.* [21].

The B_{2g} symmetry presents two clear resonances in the elastic cross section that have mixed shape core-excited character as evidenced by the shifting of their positions we observe between models. In the inelastic cross section, it is possible to observe a third broad feature centered slightly above 7 eV that we cannot conclusively identify as a physical resonance: the corresponding feature in the time-delay would be very wide and low and may be hidden by the presence of other features. Three resonances of this symmetry are identified by Cheng *et al.*: a shape one at 5.5 eV and two core-excited ones at 4.410 and 5.910 eV. The widths of these resonances are very different to ours (see Table 3). Since the authors used two different methods to identify shape and core-excited resonances, we think it is possible they observed the same (mixed character) resonance at two different energies.

The bound state of p-BQ$^-$ has B_{2g} symmetry. For the neutral geometry of p-BQ, West *et al.* positioned the bound state 1.48 eV below the ground state whereas Kunitsa and Bravaya locate it 1.75 eV below it. The lowest R-matrix pole for the corresponding symmetry, which gives a reasonable estimate of the bound state energy, is 1.57eV below the ground state.

The B_{3g} symmetry presents no pure shape resonances. The barely visible structure at 1.75 eV in the elastic CC cross section, also just about visible in the time-delay for this calculation, corresponds to the resonance reported in Table 2 and its narrow width indicates that it is likely a Feshbach resonance. The other peak in the SEP cross section (at around 7 eV) is almost certainly a pseudoresonance. The CC time-delay shows two clear resonances at 5.12 eV and 7.05 eV (the other structure corresponds to thresholds). Despite the fact that no peak-like feature is visible in the inelastic cross section, we identify these as physical resonances.

The last symmetry is the A_u. The lowest energy resonance for the system, of pure shape character, has this symmetry and is reported in Table 2. The CC calculations also show the presence of three core-excited resonances at 6.99, 7.31 and 7.62 eV, clearly visible in both inelastic cross section and time-delay.

Table 3 lists the resonance positions obtained by Cheng's *et al.* mainly from simpler calculations than those used for the data quoted in Table 2 (three resonances identified by them are not included in this table as they do not correspond to any of ours). The matching between their and our resonances has been done on symmetry and energy order. The disagreement between ours and their results is significant, both in terms of the absolute and relative position of the resonances. We expect our calculations to overestimate the position of the resonances and, indeed, most of Cheng's *et al.*'s appear at lower energies. In addition, it is possible that we may have missed some Feshbach resonances that, being very narrow and close to an excitation threshold, are very hard to spot in either the cross section or the time-delay.

As stated before, the parent states of the resonances were determined by the branching ratios obtained from the time-delay analysis. This was based on the assumption that, given their widths, the resonances are not of Feshbach character. Our character assignation is consistent with that of Cheng *et al.* except for one resonance that appears in our calculation at 7.08 eV and that we deem core-excited shape whereas they identify it as of mixed character. In terms of the parent states of the resonances, we find agreement for some of the resonances but not others as can be seen from Table 3.

5 Conclusions

We have presented both elastic and inelastic scattering calculations for *para*-benzoquinone, in the 0-8 eV energy range. These calculations have enabled us to investigate the resonance spectrum of p-BQ in greater detail than ever before, as well as determine the integral elastic and inelastic cross sections for this

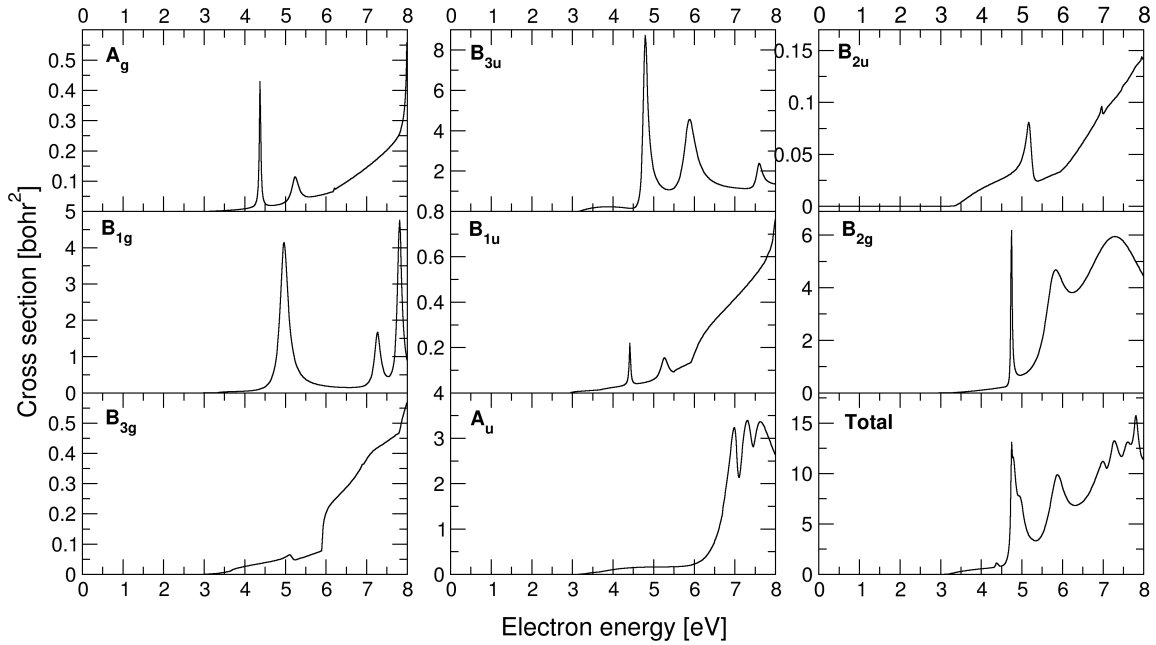

Fig. 4 Contributions to the total inelastic cross section from the scattering symmetries indicated in the panels. The bottom right hand panel shows the total inelastic cross sections (sum of all symmetry contributions) for excitation into all the excited states included in our calculation.

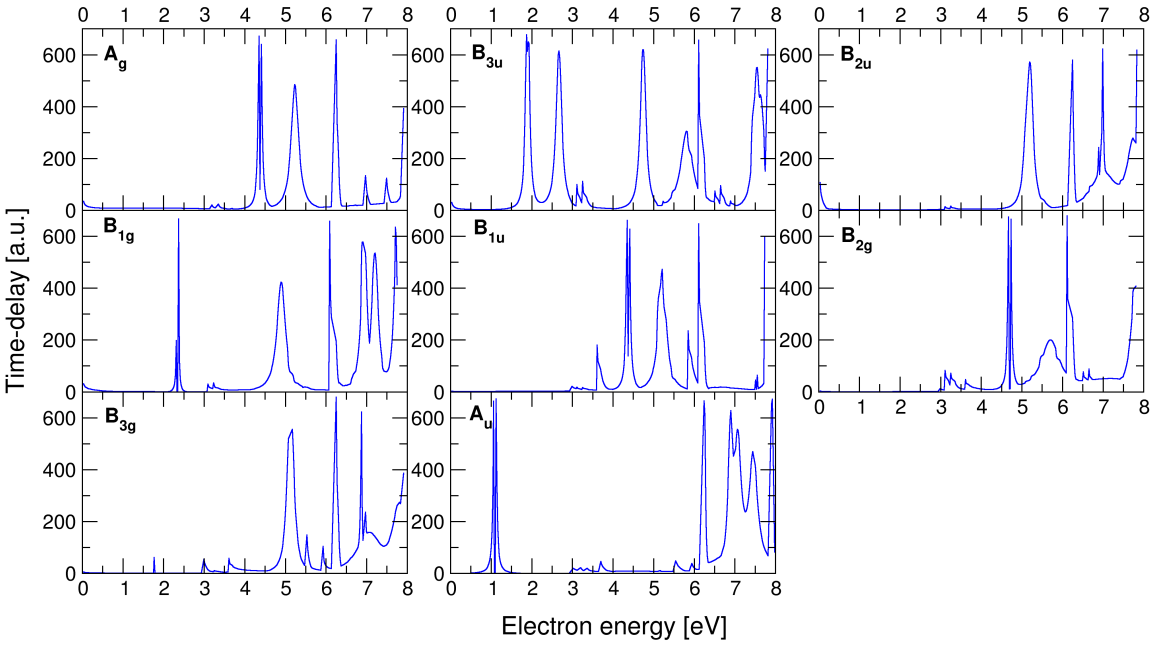

Fig. 5 Eigenvalues of the time-delay matrix for the scattering symmetries indicated in the panels at CC level for the same parameters as in Figure 4. Note that most sharp peaks (that normally appear in more than one symmetry) correspond to thresholds.

Table 3 Positions and widths (in eV), and character of the resonances found in our CC calculations as well as their most likely parent state(s). The capital letters mean: M, mixed shape core-excited; CE, core-excited shape. Earlier theoretical data: Cheng *et al.*[21] (most results quoted are those from their non-averaged calculation; for the 1^2B_{2g} and 2^2B_{2g} resonances we also quote the positions and widths from their Table 3) , West *et al.*[18]. Experimental position of first $^2B_{2g}$ resonance: Modelli and Burrow[27], Allan[28].

Symm.	E_R (Width)	Char.	Most likely P.S.	Cheng *et al.*/other	P.S. (Cheng's)
1^2A_g	4.37 (0.041)	CE	1^1A_u, 1^3A_u, 1^1B_{1g}	3.69	A_u, B_{2g}, B_{2u}
1^2B_{1u}	4.41 (0.043)	CE	1^1B_{1g}, 1^3B_{1g}, 1^1A_u	3.37	B_{3u}, B_{1g}, B_{2u}
1^2B_{2g}	4.74 (0.032)	M	g.s., 1^3B_{3g}	4.24/4.410 (0.397) 4.37[27] 4.24[28]	g.s., A_g, B_{1u}
3^2B_{3u}	4.81 (0.133)	M	g.s., 1^3A_u, 1^3B_{3g}	3.58 2.4[18]	g.s., B_{3g}, B_{2u}, B_{1u}
2^2B_{1g}	4.97 (0.238)	M	g.s., 2^3B_{1u}	4.14	g.s., B_{2u}, B_{1u}, B_{3g}
2^2B_{3g}	5.10 (0.147)	CE	1^1A_u, 1^3A_u, 1^1B_{1g}	4.30	A_u, B_{1u}, B_{1g}
2^2B_{2u}	5.16 (0.169)	CE	1^3B_{1g}, 1^1B_{1g}, 2^3B_{1u}	3.97	A_u, B_{1u}, B_{1g}
2^2A_g	5.24 (0.189)	CE	1^1A_u, 1^3A_u, 1^3B_{1g}	4.06	A_u, B_{2u}, B_{2g}
2^2B_{1u}	5.27 (0.137)	CE	1^3B_{1g}, 1^1B_{1g}	3.82	B_{2u}, B_{3u}, B_{1g}
2^2B_{2g}	5.76 (0.526)	M	g.s., 2^3B_{1u}	5.92/5.910 (0.375)	g.s., B_{1u}
4^2B_{3u}	5.95 (0.316)	M	g.s., 1^3B_{3g}	5.46	g.s., B_{2u}, B_{1u}, B_{3g}
3^2B_{2u}	6.96 (0.039)	CE	1^1A_u, 1^3B_{1g}, 2^1B_{1g}	4.88	A_u, B_{1g}, B_{1u}
2^2A_u	6.99 (0.142)	CE	2^3B_{1u}, 3^3B_{1u}	5.41	B_{2u}, B_{3g}, B_{1u}
3^2B_{3g}	7.08 (0.71)	CE	1^3B_{1g}, 1^1B_{1g}	4.64	g.s., B_{1g}
3^2B_{1g}	7.29 (0.186)	CE	1^3B_{3u}	5.12	B_{2u}, B_{1u}, B_{3g}
3^2A_u	7.31 (0.249)	CE	2^3B_{1u}, 3^3B_{1u}	-	-
5^2B_{3u}	7.62 (0.172)	CE	1^3B_{3g}, 1^1B_{3g}, 2^1A_g	5.87	g.s., B_{2u}, B_{1u}, B_{3g}
4^2A_u	7.62 (0.300)	CE	2^3B_{1u}, 3^3B_{1u}, 1^A_u	-	-
4^2B_{1g}	7.79 (0.096)	M	g.s., 1^3B_{1u}	-	-

target.

We have identified a large number of resonances, mainly of core-excited and mixed character. Most of these resonances appear above 4 eV, in the same energy region as a large number of excited states of *p*-BQ. The characteristics of many of these resonances had been investigated by Cheng *et al.*[21].

The six lowest resonances are in good agreement with the published data. These resonances are energetically very close (roughly within 1.5 eV) and their order around the equilibrium geometry of the neutral molecule is very sensitive to small changes in bond-lengths. We believe this may be one of the reasons why different authors have provided different orderings and, for some resonances, different character. Our results agree with those of Kunitsa and Bravaya, although their identification of the first resonance of $^2B_{3u}$ symmetry as of mixed character contradicts our analysis that this is a shape resonance. This ordering, or more generally the relative position of the resonant states, has implications for the photodetachment process. Further work, particularly experimental electron scattering measurements (e.g. electron energy loss spectroscopy and velocity map imaging experiments), could contribute to elucidating the details of the resonant spectrum for this very interesting and fundamental molecule. Future theoretical work is planned on the *p*-BQ-H_2O complex: action spectroscopy experiments[53] on *p*-BQ and *p*-BQ-H_2O have indicated that hydrogen bonding with one water molecule seems to have little effect on the photodetachment processes.

6 Acknowledgements

This work used the ARCHER UK National Supercomputing Service (http://www.archer.ac.uk). It was supported by Fundação para a Ciência e a Tecnologia (FCT-MCTES), Radiation Biology and Biophysics Doctoral Training Programme (RaBBiT, PD/00193/2012); UID/Multi/04378/2013 (UCIBIO); UID/FIS/00068/2013 (CEFITEC); and scholarship grant number SFRH/BD/106031/2015 to A Loupas. This work was conducted within the framework of the COST Action CM1301 (CELINA).

References

1 I. Baccarelli, I. Bald, F. A. Gianturco, E. Illenberger and J. Kopyra, *Phys. Rep.*, 2011, **508**, 1–44.
2 B. Boudaïffa, P. Cloutier, D. Hunting, M. A. Huels and L. Sanche, *Science*, 2000, **287**, 1658.
3 J. D. Gorfinkiel and S. Ptasińska, *J. Phys. B*, submitted.
4 R. Doong, C. Lee and C. Lien, *Chemosphere*, 2014, **97**, 54.
5 B. Huskinson, M. Markshak, C. Suh, S. Er, M. Gerhardt, C. Galvin, X. Chen, A. Aspuru-Guzik, R. Gordon and M. Aziz, *Nature*, 2014, **505**, 195.
6 H. Nohl, W. Jordan and R. J. Youngman, *Adv. Free Radical Bio.*, 1986, **2**, 211 – 279.
7 J. Lown, *Chemical Society Reviews*, 1993, **22**, 165.
8 M. Colucci, G. Couch and C. Moody, *Organic Biomolecular Chemistry*, 2008, **6**, 637.
9 K. Klinman and D. Mu, *Annual Reviews of Biochemistry*, 1994, **63**, 299.
10 T. Stites, A. Mitchell and R. Rucker, *Journal of Nutrition*, 2000,

130, 719.
11 A. Cook, L. Curtiss and J. Miller, *Journal of American Chemical Society*, 1997, **119**, 5729.
12 M. Zamadar, A. Cook, A. Lewandowska-Andralojc, R. Holroyd, Y. Jiang, J. Bikalis and J. Miller, *Journal of Physical Chemistry A*, 2013, **117**, 8360.
13 R. Holroyd, *Journal of Physical Chemistry*, 1982, **86**, 3541.
14 K. Strode and E. Grimsrud, *Chemical Physics Letters*, 1994, **229**, 551.
15 N. Asfandiarov, S. Pschenichnyuk, A. Fokin and E. Nafikova, *Chemical Physics*, 2004, **298**, 263.
16 J. Schiedt and R. Weinkauf, *The Journal of Chemical Physics*, 1999, **110**, 304.
17 D. A. Horke, Q. Li, L. Blancafort and J. R. R. Verlet, *Nat. Chem.*, 2013, **5**, 711–717.
18 C. West, J. Bull, E. Antonkov and J. Verlet, *The Journal of Physical Chemistry A*, 2014, **118**, 11346.
19 R. Pou-Amérigo, L. Serrano-Andrés, M. Merchán, E. Ortí and N. Forsberg, *Journal of American Chemical Society*, 2000, **122**, 6067.
20 Y. Honda, M. Hada, M. Ehara and H. Nakatsuji, *Journal of Physical Chemistry A*, 2002, **106**, 3838.
21 H. Cheng and Y. Huang, *Physical Chemistry Chemical Physics*, 2014, **16**, 26306.
22 A. Kunitsa and K. Bravaya, *The Journal of Physical Chemistry Letters*, 2015, **6**, 1053.
23 A. Kunitsa and K. Bravaya, *Physical Chemistry Chemical Physics*, 2016, **18**, 3454.
24 C. Cooper, W. Naff and R. Compton, *Journal of Chemical Physics*, 1995, **63**, 2752.
25 M. Allan, *Chemical Physics*, 1983, **81**, 235.
26 L. Christophorou, J. Carter and A. Christodoulides, *Chemical Physics Letters*, 1969, **3**, 237.
27 A. Modelli and P. D. Burrow, *Journal of Physical Chemistry*, 1984, **88**, 3550.
28 M. Allan, *Chemical Physics*, 1984, **84**, 311.
29 M. Ghazali, A. Svendsen, H. Bluhme, S. Nielsen and L. Andersen, *Chemical Physics Letters*, 2005, **405**, 278.
30 P. G. Burke, *R-Matrix Theory of Atomic Collisions: Application to Atomic, Molecular and Optical Processes*, Springer, 2011.
31 J. Tennyson, *Physical Reports*, 2010, **491**, 29.
32 J. M. Carr, P. G. Galiatsatos, J. D. Gorfinkiel, A. G. Harvey, M. A. Lysaght, D. Madden, Z. Mašín, M. Plummer, J. Tennyson and H. N. Varambhia, *The European Physical Journal D*, 2012, **66**, 58.
33 J. Tennyson, *Journal of Physics B: Atomic, Molecular and Optical Physics*, 1996, **29**, 6185.
34 A. U. Hazi, *Physical Reviews A*, 1979, **19**, 920.
35 Z. Mašín and J. Gorfinkiel, *The Journal of Chemical Physics*, 2012, **137**, 144308.
36 F. T. Smith, *Physical Reviews*, 1960, **118**, 349.
37 R. D. Johnson III Editor, *NIST Standard Reference Database Number 101*, 2011.
38 M. Dewar and S. Worley, *The Journal of Chemical Physics*, 1969, **60**, 654.
39 M. Gussoni, R. Rui and G. Zerbi, *Journal of Molecular Structure*, 1998, **447**, 163.
40 R. Pou-Amérigo, M. Merchán and E. Ortí, *The Journal of Chemical Physics*, 1999, **110**, 9536.
41 M. Alipour, *Theoretical Chemistry Accounts*, 2015, **134**,.
42 J. Weber, K. Malsch and G. Hohlneicher, *Chemical Physics*, 2001, **264**, 275.
43 M. Schreiber, M. Silva-Junior, S. Sauer and W. Thiel, *The Journal of Chemical Physics*, 2008, **128**, 134110.
44 H.-J. Werner, P. J. Knowles, G. Knizia, F. R. Manby, M. Schütz, P. Celani, W. Györffy, D. Kats, T. Korona, R. Lindh, A. Mitrushenkov, G. Rauhut, K. R. Shamasundar, T. B. Adler, R. D. Amos, A. Bernhardsson, A. Berning, D. L. Cooper, M. J. O. Deegan, A. J. Dobbyn, F. Eckert, E. Goll, C. Hampel, A. Hesselmann, G. Hetzer, T. Hrenar, G. Jansen, C. Köppl, Y. Liu, A. W. Lloyd, R. A. Mata, A. J. May, S. J. McNicholas, W. Meyer, M. E. Mura, A. Nicklass, D. P. O'Neill, P. Palmieri, D. Peng, K. Pflüger, R. Pitzer, M. Reiher, T. Shiozaki, H. Stoll, A. J. Stone, R. Tarroni, T. Thorsteinsson and M. Wang, *MOLPRO, version 2015.1, a package of ab initio programs*, 2015, see http://www.molpro.net.
45 M. Koyanagi, Y. Kogo and Y. Kanda, *Molecular Physics*, 1971, **20**, 747.
46 M. Koyanagi, Y. Kogo and Y. Kanda, *Journal of Molecular Spectroscopy*, 1970, **34**, 450.
47 M. Hollas, *Spectrochimica acta*, 1964, **20**, 1563.
48 G. T. Horst and J. Kommandeur, *Chemical Physics*, 1979, **44**, 287.
49 H. P. Trommsdorff, *Journal of Chemical Physics*, 1972, **56**, 5358.
50 P. Brint, J.-P. Connerade, P. Tsekeris, A. Bolovinos and A. Baig, *Journal of Chemical Society, Faraday Trans 2*, 1986, **82**, 367.
51 A. Faure, J. D. Gorfinkiel, L. A. Morgan and J. Tennyson, *Comp. Phys. Commun.*, 2002, **144**, 224–241.
52 Z. Mašín and J. D. Gorfinkiel, *The Journal of Chemical Physics*, 2011, **135**, 144308.
53 M. H. Stockett and S. B. Nielsen, *Phys. Chem. Chem. Phys.*, 2016, **18**, 6996–7000.